Research on the rapid diagnosis method for hunting of high-speed trains

Wanru Xie
Infrastructure Inspection Research Institute, China Academy of Railway Sciences Corporation Limited, Beijing, China
Yixin Zhao and Gang Zhao
Infrastructure Inspection Center, China Railway Corp, Beijing, China
Fei Yang and Zilong Wei
Infrastructure Inspection Research Institute, China Academy of Railway Sciences Corporation Limited, Beijing, China, and
Jinzhao Liu
Infrastructure Inspection Institute, China Academy of Railway Sciences Corporation Limited, Beijing, China

Received 18 October 2024
Revised 4 December 2024
Accepted 18 December 2024

Abstract

Purpose – High-speed turnouts are more complex in structure and thus may cause abnormal vibration of high-speed train car body, affecting driving safety and passenger riding experience. Therefore, it is necessary to analyze the data characteristics of continuous hunting of high-speed trains passing through turnouts and propose a diagnostic method for engineering applications.

Design/methodology/approach – First, Complete Ensemble Empirical Mode Decomposition with Adaptive Noise (CEEMDAN) is performed to determine the first characteristic component of the car body's lateral acceleration. Then, the Short-Time Fourier Transform (STFT) is performed to calculate the marginal spectra. Finally, the presence of a continuous hunting problem is determined based on the results of the comparison calculations and diagnostic thresholds. To improve computational efficiency, permutation entropy (PE) is used as a fast indicator to identify turnouts with potential problems.

Findings – Under continuous hunting conditions, the PE is less than 0.90; the ratio of the maximum peak value of the signal component to the original signal peak value exceeded 0.7, and there is an energy band in the STFT time-frequency map, which corresponds to a frequency distribution range of 1–2 Hz.

Originality/value – The research results have revealed the lateral vibration characteristics of the high-speed train's car body during continuous hunting when passing through turnouts. On this basis, an effective diagnostic method has been proposed. With a focus on practical engineering applications, a rapid screening index for identifying potential issues has been proposed, significantly enhancing the efficiency of diagnostic processes.

Keywords High-speed railway, Periodic hunting, Rapid diagnosis, CEEMDAN, STFT, Permutation entropy

Paper type Research paper

1. Introduction

High-speed turnouts are one of the important yet fragile pieces of equipment in high-speed railway track systems; therefore, their usage status must be evaluated in real time to ensure the safety of high-speed EMUs as they pass through turnouts (Kaewunruen, 2014; Li, Ding, Li,

The financial support from the funds of National Natural Science Foundation of China (52308473) and China Academy of Railway Science Corporation Limited (2022YJ192) are gratefully acknowledged.

Railway Sciences
Vol. 4 No. 1, 2025
pp. 1-21
Emerald Publishing Limited
e-ISSN: 2755-0915
p-ISSN: 2755-0907
DOI 10.1108/RS-10-2024-0042

Niu, & Yang, 2020; Wang, Wang, Ge, Si, & Yang, 2023). Currently, there are two primary methods to assess the usage status of turnouts: manual assessment and assessment using high-speed comprehensive inspection vehicles. The manual method involves professional technical personnel entering the turnout section to be evaluated, using professional measurement tools to assess the track system parameters, such as the track geometry of the turnout section, under no external load. This method can reflect the static state of the turnout system, but cannot reflect the vibration state of the high-speed train as it passes through the turnout. Dependent on professional technical personnel and their experience, this evaluation method has low efficiency and exhibits significant variations in the quality of the evaluation results. In contrast to passenger multiple units, high-speed comprehensive inspection vehicles (Li *et al.*, 2021; Niu, 2020) are equipped with special inspection equipment. They assess the track system parameters, including the track geometry of the turnout section, under external loads, and can also measure the vibration information at the axle box, bogie, and car body positions when the inspection vehicle passes through (Zhang *et al.*, 2021; Niu *et al.*, 2020). These detection data can help to understand the true dynamic characteristics of the high-speed vehicle and turnout system (Xie, 2022; Cheng *et al.*, 2024; Cong *et al.*, 2024).

When high-speed EMUs pass through the turnout, the contact points between the wheelset and the track are not continuous. Some sections are in contact with the switch rail, while others are in contact with the basic rail. Therefore, compared to the main line, the vibration characteristics of the vehicle in the turnout section are more complex, especially the lateral vibration (Wang, 2016; Shi *et al.*, 2022). As usage time increases, the switch point position will also experience wear, which can have an adverse impact on the passing performance of the high-speed EMUs (Wang, Wang, Ge, Si, & Yang, 2022; Yang, Wang, Sun, & Wang, 2020; Gao, Si, Wang, & Yang, 2023). In addition, whether the reduction value of the switch point is within a reasonable range directly affects the dynamic characteristics of the high-speed vehicle and turnout system (Ma, Wang, Wang, & Xu, 2016; Wang, Si, Wang, & Ge, 2014). If the reduction value of the switch point is not reasonable, there will be a difference in the diameter of the wheelset, causing the left and right wheels to roll forward with different radii. The wheelset will then hunt, and due to the low vibration frequency, the hunting motion will also be transmitted to the car body, causing a rapid decrease in the lateral stability of the high-speed EMU.

Although there has been no targeted research on the periodic hunting problem of turnout sections, the hunting motion problem is an eternal dynamic problem in the field of railway vehicles (Luo & Shi, 2018; Wei, 2016), and the related research is abundant, providing experience for conducting hunting evaluation of turnout sections. Chi, Zhang, Zeng, Jin, and Zhu (2008) conducted a theoretical analysis and found that the car body's low-frequency periodic hunting is caused by the bogie motion's frequency approaching the car body's natural frequency. Sun, Wang, Liu, and Li (2012) studied the problem of vehicle hunting by establishing a vehicle system dynamics simulation model. When the speed is 200 km/h, the vibration frequency of the center roll vibration mode on the car body of the constructed model is 1.6 Hz, and the damping factor is negative and very close to 0, resulting in slow attenuation of the center roll vibration and causing hunting. Liu (2016) studied the influence of primary and secondary suspension parameters on car body hunting through online experiments. The research provides theoretical support for understanding and identifying hunting phenomena.

Based on these findings, researchers further explore the causes of hunting and propose identification methods by the introduction of time-frequency analysis techniques. Some new methods were proposed to address the issue of hunting for high-speed train, which combines ensemble empirical mode decomposition (EEMD), entropy features and least squares support vector machine (LSSVM) (Ye, Ning, Zhong, Cui, & Liu, 2016, 2017). Xie *et al.* (2022) proposed a method for identifying low-frequency periodic hunting based on frequency characteristics. However, this method requires determining the distribution range of the main vibration frequency based on the actual technical parameters of the high-speed EMUs. Although the results obtained are accurate, the method loses its recognition ability when the

technical parameters are unknown. Xia, Zhou, Gong, Sun, and Sun (2018) conducted a vibration mode similarity test using relevant distance indicators and concluded that using vibration mode similarity as an indicator to diagnose low-frequency hunting is feasible. Deng, Zhou, Xia, Gong, and Sun (2020) employed Empirical Mode Decomposition (EMD) and Hilbert Transform to extract features from measured hunting signals and defines the spectral energy ratio as a detection index to measure vibration energy characteristics. However, this approach is not sensitive to critical states. Sun *et al.* (2021) analyzed the degree of cross-correlation between acceleration information at different positions and found that it can be used to identify the small amplitude hunting ability of high-speed vehicles. This method requires the simultaneous acquisition of lateral accelerations for both the bogie and the car body of the same carriage. The usability of the method will be greatly reduced when there is a lack of data. Additionally, if the sensor''s installation position is not reasonable, the accuracy of the recognition results will decrease. Ye, Ning, Zhong, Cui, and Chen (2018) employed the Modified Ensemble Empirical Mode Decomposition (MEEMD) to decompose the bogie's vibration signals in three distinct states: normal, critical and hunting instability. The energy characteristics of the resulting Intrinsic Mode Functions (IMFs) were then fed into the Least Squares Support Vector Machine (LSSVM) for training purposes. This led to the development of a MEEMD-LSSVM model capable of predicting the bogie's hunting instability. The model was designed to analyze hunting instability in specific types of high-speed trains operating at speeds between 330 and 350 km/h. Further research is required to assess the accuracy of this method across various vehicle models and speeds. Ning *et al.* (2018) proposed a feature extraction method based on Multiscale Permutation Entropy (MPE) and Local Tangent Space Alignment (LTSA), which was proposed to extract features of the small amplitude hunting signals. Ye and Ning (2019) considered that the small-amplitude hunting signals had strong nonlinear characteristics, and their frequency and amplitude were unstable, so a new feature extraction method based on the independent mode function reconstruction and linear local tangent space alignment (IMFR-LLTSA) was proposed. Guo, Zhang, Shi, and Zeng (2023) combined the spectral frequency spread and autocorrelation coefficient with a decision tree algorithm to identify low-amplitude hunting instability, with a success rate of 99.94%. Wang, Ning, Zhao, Li, and Chen (2023) employed an energy-based technique for diagnosing hunting instability by utilizing the Hilbert-Huang Transform (HHT). This method not only enabled a qualitative evaluation of hunting motion in high-speed trains by examining the dominant frequency magnitude, spectral concentration, and frequency values, but also offered a quantitative assessment of the degree of hunting instability. At present, China has built the world's largest high-speed railway network. Effectively detecting and monitoring the status of railway infrastructure, accurately locating problem areas, and carrying out precise maintenance have become hot and key research issues. When hunting occurs, the car body's lateral acceleration exhibits amplitude increases and periodic characteristics. According to the literature review, it is known that current research on hunting monitoring methods has the drawback of low computational efficiency, which cannot meet the requirements of online engineering applications. This paper takes the car body's lateral acceleration as the research object, which is collected by sensors installed on the floor of the high-speed comprehensive inspection vehicle. Considering that the car body's lateral acceleration is a non-stationary signal, the signal is subjected to CEEMDAN to obtain the typical feature components. Then, these typical feature components are subjected to STFT, and the marginal spectrum is calculated to accurately extract the lateral vibration amplitude and periodic characteristics.

This paper is organized as follows: Section 2 provides a mathematical introduction to CEEMDAN, STFT, and PE. Section 3 presents a method for identifying hunting using a combination of CEEMDAN and STFT. Section 4 explores the influence of parameters on PE and provides PE values that can rapidly identify possible hunting signals. In Section 5, the proportion of hunting is obtained by analyzing the car body's lateral acceleration of a typical high-speed vehicle using the proposed method.

2. Methodology

2.1 Complete ensemble empirical mode decomposition with adaptive noise (CEEMDAN)

The EMD algorithm is proposed by Huang *et al.* (1998), which decomposes the complex original signal into a series of IMFs with different amplitude and a residual. Its essence is the transition from nonlinear and non-stationary signals to linear and stationary.

The EEMD method can solve the modal aliasing of the EMD algorithm by adding different white noises to the original sequence (Wu & Huang, 2009). However, the noise sequence added by the EEMD method is not completely offset by a finite amount of averaging. The size of the reconstructed error depends on the number of integration, although it can be reduced gradually with the increase of the average number of iterations; however, the computations increased the time consumption. CEEMDAN algorithm adds finite adaptive white noise based on EEMD, and overcomes the problems of EEMD's incompleteness and reconstruction error after adding white noise (Torres, Colominas, Schlotthauer, & Flandrin, 2011). Therefore, the CEEMDAN overcomes the mode mixing in the EMD, and solves the problem of the EEMD, which is its incomplete decomposition and low computational efficiency caused by increasing the number of integration to reduce the reconstruction error.

The details of the algorithm for the mode component generated by the CEEMDAN (recorded as IMF_k) are as follows:

Step 1: Add white noise $v^i(t)$ with a standard normal distribution to the original signal $S(t)$. The signal for the ith to calculate the first modal component is represented as formula (1).

$$S_1{}^i(t) = S(t) + e_0 E_1\left(v^i(t)\right), i = 1, 2, ..., I. \tag{1}$$

where e_0 is signal-to-noise ratio, E_1 is the the first Intrinsic mode component generated through the EMD algorithm, $v^i(t)$ is the white noise sequence following standard normal distribution added for the ith time

Step 2: The signals obtained in step 1 are subjected to EMD decomposition and the first modal component is obtained, which is represented as formula (2).

$$\mathrm{IMF}_1(t) = \frac{1}{I}\sum_{i=1}^{I} \mathrm{IMF}_1^i(t) \tag{2}$$

Step 3: In the first stage ($k = 1$), the first unique residual sequence is calculated:

$$r_1(t) = S(t) - \mathrm{IMF}_1(t) \tag{3}$$

Step 4: The new signals are constructed as Equation (4) for obtaining the mth modal component.

$$S_m{}^i(t) = r_{m-1}(t) + e^{m-1}E_m\left(v^i(t)\right), i = 1, 2, ..., I. \tag{4}$$

Step 5: The signals obtained in step 4 is subjected to EMD decomposition and the mth modal component is obtained, which is represented as formula (5).

$$\mathrm{IMF}_m(t) = \frac{1}{I}\sum_{i=1}^{I} IMF_1^i(t) \tag{5}$$

Step 6: For each of the remaining stages ($m = 2, \ldots, n$), calculate the mth residual sequence; consistent with the calculation in step 3, calculate the mth mode components as follows:

$$r_m(t) = r_{m-1}(t) - \mathrm{IMF}_m(t) \tag{6}$$

When the residual $r_n(t)$ is monotony functions and cannot be decomposed by EMD, the program terminates. The original signal can be represented as formula (7).

$$S(t) = \sum_{i=1}^{n} \mathrm{IMF}_i + r_n(t) \tag{7}$$

2.2 Short-Time Fourier Transform (STFT) and marginal spectrum

Short-time Fourier transform (STFT) is widely used to find the time-frequency representations of local sections of time-varying signals using a time window function (Garrido, 2016). The STFT of the input signal $S(t)$ is represented as

$$STFT(t,f) = \int_{-\infty}^{\infty} S(\tau) w(\tau - t) e^{-j2\pi f\tau} d\tau \tag{8}$$

where $w(t)$ is the window function, t is the translation parameter, τ represents time delay.

The calculation of marginal spectrum is based on formula (9)

$$MS(f) = \sum_{t=0}^{T} STFT(t,f) \tag{9}$$

where T is the time scale of time series.

2.3 Permutation entropy (PE)

PE is used to measure the randomness and detect the dynamic changes of the time series (Kang, Zhang, & Zhang, 2020). It is designed based on the comparison of the adjacent values in the time series, and its definition and calculation steps are briefly summarizes as follows (Zheng, Pan, Yang, & Cheng, 2018).

For a time series length $N\{x(k), k = 1, 2, \ldots, N\}$, the m-dimensional vector at time i can be constructed as

$$X_i^m = \{x(i), x(i+\tau), ..., x(i+(m-1)\tau)\}, i = 1, 2, ..., N-(m-1)\tau \tag{10}$$

where X_i^m is a new time series, m is the embedding dimension, and τ is the time delay.

As described in article (Kang *et al.*, 2020), the X_i^m has a permutation $\pi_{r_0, r_1, \ldots, r_{m-1}}$ when X_i^m satisfies the following condition

$$x(t + r_0\tau) \le x(t + r_1\tau) \le \ldots \le x(t + r_{m-1}\tau) \tag{11}$$

where $0 \le r_1 \le m-1$ *and* $r_i \ne r_j$.

It can be shown in formula (11) that a m-tuple vector has $m!$ possible distributions. In addition, the relative frequency of each distribution is defined as

$$P(i) = \frac{Num\{X_i^m\}}{N-(m-1)\tau} \tag{12}$$

where $Num\{X_i^m\}$ indicates the number of X_i^m, and it is consistent with the type π.

Therefore, the PE with m dimensions can be described as formula (13).

$$H_{PE}(m) = -\sum_{i}^{N-(m-1)\tau} P(i)\ln(P(i)) \tag{13}$$

It should be noted that when $P(i) = 1/m!$, H_{PE} reaches the maximum value $\ln(m!)$. The PE values can be normalized through $\ln(m!)$. as

$$H_{NPE}(m) = H_{PE}(m)/\ln(m!) \tag{14}$$

More specifically, the value of $H_{NPE}(m)$ is within the range from 0 to 1.

It can be seen that the smaller the H_{NPE} value is, the more periodic and regular the time series is. On the other hand, a larger H_{NPE} value means that the time series is more irregular and random. When the time series is white noise, the H_{NPE} value is equal to 1. For the sine or cosine signals, the value of H_{NPE} equals 0. Therefore, PE can be applied to estimate the complexity and dynamic changes of the signals.

3. Method for diagnosing periodic hunting in turnout area

The design length of the 1/18 high-speed turnout is 69 m. To ensure that the partial vibration characteristics of the high-speed train both before and after traversing the turnout are fully captured and preserved, the lateral acceleration data extraction length for the vehicle body is set to encompass a total of 229 m. This distance is broken down as follows: 80 m preceding the turnout, the entire 69-m length of the turnout itself, and an additional 80 m beyond the turnout. This comprehensive approach ensures that the vibration data is collected from a sufficient distance before and after the turnout to analyze the train's behavior through the transition (Qin, Liu, Wang, & Sun, 2019; Xie *et al.*, 2024).

3.1 Decomposed by CEEMDAN

Figure 1 (a) and (b) are the waveforms of the car body's lateral acceleration for the hunting and no hunting state in the turnout area.

Perform CEEMDAN on the above signals separately, and the results are shown in Figure 2. From Figure 2 (a) and (b), the car body's lateral acceleration of the hunting is decomposed into

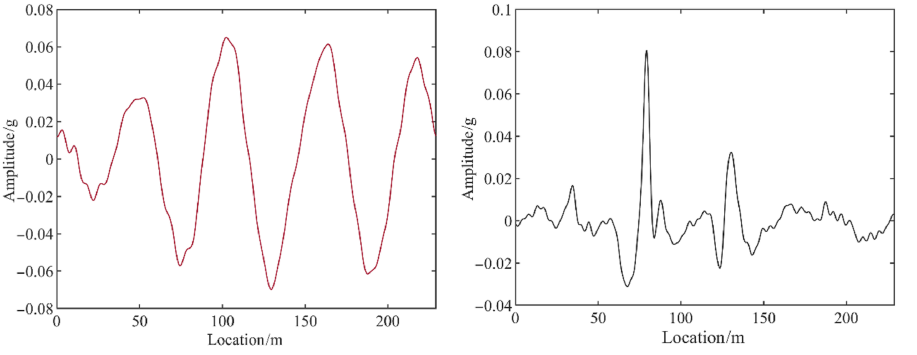

Source(s): Authors' own work

Figure 1. The carbody's lateral acceleration

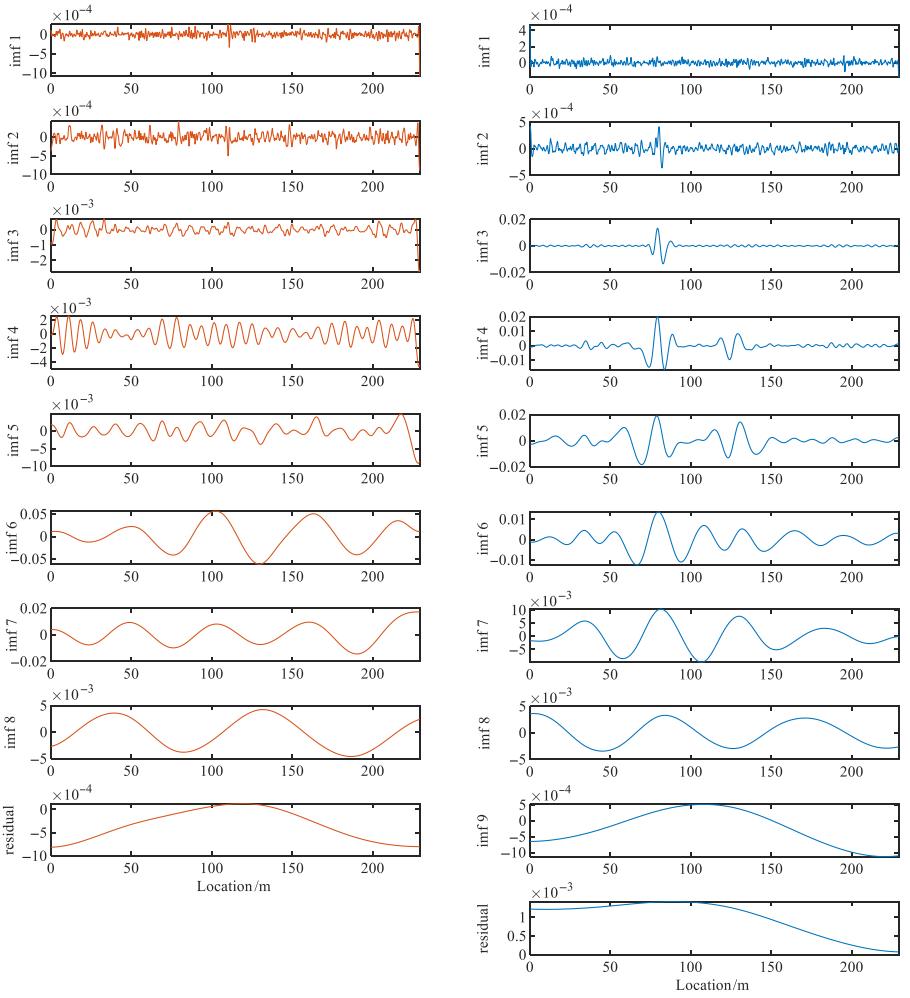

Hunting **No Hunting**

(a) **(b)**

Source(s): Authors' own work

Figure 2. The result of CEEMDAN

8 signal components, while the car body's lateral acceleration of the no hunting is decomposed into 9 signal components. This indicates that there is a significant difference in the frequency composition of the two signals.

Table 1 shows the peak values and standard deviations of each signal component.

For the hunting, the maximum peak value is 0.05697 g, which is from IMF6; the maximum standard deviation is 0.03158 g, which is also from IMF6. For the no hunting, the maximum peak value is 0.02013 g, which is from IMF4; the maximum standard deviation is 0.00577 g, which is from IMF5.

The signal component with the maximum peak is referred to as the first feature component, and the signal component with the maximum standard deviation is referred to as the second

Table 1. The peak values and standard deviations of each signal component

Signal component	Hunting Peak value	Standard deviations	No hunting Peak value	Standard deviations
imf 1	0.00029	0.00007	0.00047	0.00003
imf 2	0.00035	0.00012	0.00042	0.00007
imf 3	0.00092	0.00027	0.01337	0.00187
imf 4	0.00317	0.00119	*0.02013*	0.00379
imf 5	0.00502	0.00204	0.01903	*0.00577*
imf 6	*0.05697*	*0.03158*	0.01365	0.00463
imf 7	0.01068	0.00551	0.01038	0.00472
imf 8	0.00433	0.00285	0.00363	0.00228
imf 9	/	/	0.00052	0.00054

Source(s): Authors' own work

feature component. Analyze the quantitative relationship between them and the original signal separately, and the results are shown in Table 2.

For the hunting, the ratio of the peak value of the first feature component to the peak value of the original signal is 0.88, and the ratio of the standard deviation of the second feature component to the standard deviation of the original signal is 0.85. For the no hunting, the ratio of the peak value of the first feature component to the peak value of the original signal is 0.25, and the ratio of the standard deviation of the second feature component to the standard deviation of the original signal is 0.44. The ratio of the first and second feature components of the hunting to the original signal is significantly higher than that of the no hunting.

Calculate the peak and standard deviation of the car body's lateral acceleration of 40 sets of hunting and 40 sets of no hunting. Perform CEEMDAN, obtain the first and second feature components and calculate the ratio. The results are shown in Figure 3.

From Figure 3 (a), the peak ratio of hunting is greater than 0.7, but the peak ratio of no hunting is less than 0.6. From Figure 3 (b), the standard deviation ratios of the hunting are all greater than 0.7, with a minimum value of 0.73. The standard deviation ratios of the no hunting are mostly less than 0.7, and a few sets have larger standard deviation ratios, reaching 0.75. The peak distinguishes between hunting and no hunting more clearly.

3.2 STFT and marginal spectrum

Perform STFT on the first feature component obtained by CEEMDAN for the car body's lateral acceleration shown in Figure 1 (a) and solve for the marginal spectrum. The results are shown in Figure 4, where (a) is the first feature component, (b) is the STFT time-frequency map, and (c) is the marginal spectrum. In the time-frequency map obtained by STFT, the energy exhibits a banded distribution parallel to the *x*-axis. This indicates that the signal has a clear periodicity. The energy band is concentrated within the 2 Hz range, with the frequency at the corresponding position of the maximum edge spectrum being 1.05 Hz and the maximum edge spectrum value is close to 400 W/Hz.

Table 2. The relationship between the first/second feature components and the original signal

Type	Index	Original signal	First/Second feature	Ratio
Hunting	Peak Value	0.06495	0.05697	0.88
	Standard Deviations	0.03720	0.03158	0.85
No hunting	Peak Value	0.08052	0.02013	0.25
	Standard Deviations	0.01326	0.00577	0.44

Source(s): Authors' own work

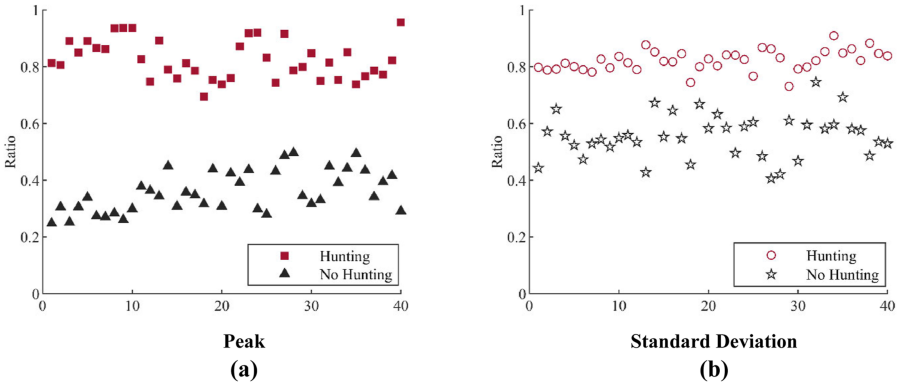

Source(s): Authors' own work

Figure 3. The ratio of feature components to the original signal

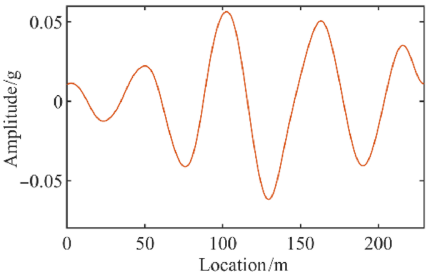

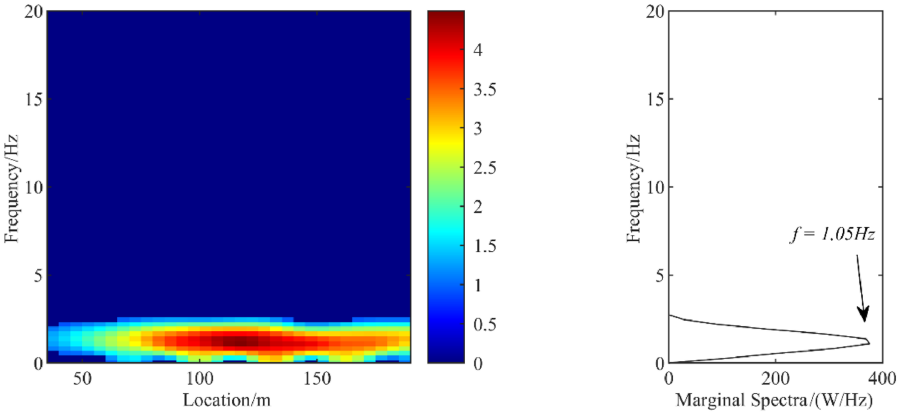

Source(s): Authors' own work

Figure 4. The STFT of hunting

Perform STFT on the first feature component obtained by CEEMDAN for the car body's lateral acceleration shown in Figure 1 (b) and solve for the marginal spectrum. The results are shown in Figure 5, where (a) is the first feature component, (b) is the STFT time-frequency map, and (c) is the marginal spectrum.

From Figure 5 (b) and (c), in the time-frequency map through STFT, the energy exhibits a clear circular distribution in the range of 70–90 m and 120–135 m. This indicates that the component contains multiple frequency components. The frequency corresponding to the maximum edge spectrum position is 4.01 Hz, and the maximum edge spectrum value is less than 2 W/Hz.

Perform SFTF on the car body's lateral acceleration of 40 sets of hunting, statistical the maximum marginal spectrum and its corresponding frequency. The result is shown in Figure 6.

From Figure 6 (a) and (b), in the hunting state, the continuous marginal spectral values are all greater than 150 W/Hz and the corresponding frequency distribution is in the range of 1–2 Hz.

3.3 Diagnostic method

Based on the above analysis, we propose a periodic hunting diagnosis method for turnout sections that combines CEEMDAN and STFT. The specific steps are as follows:

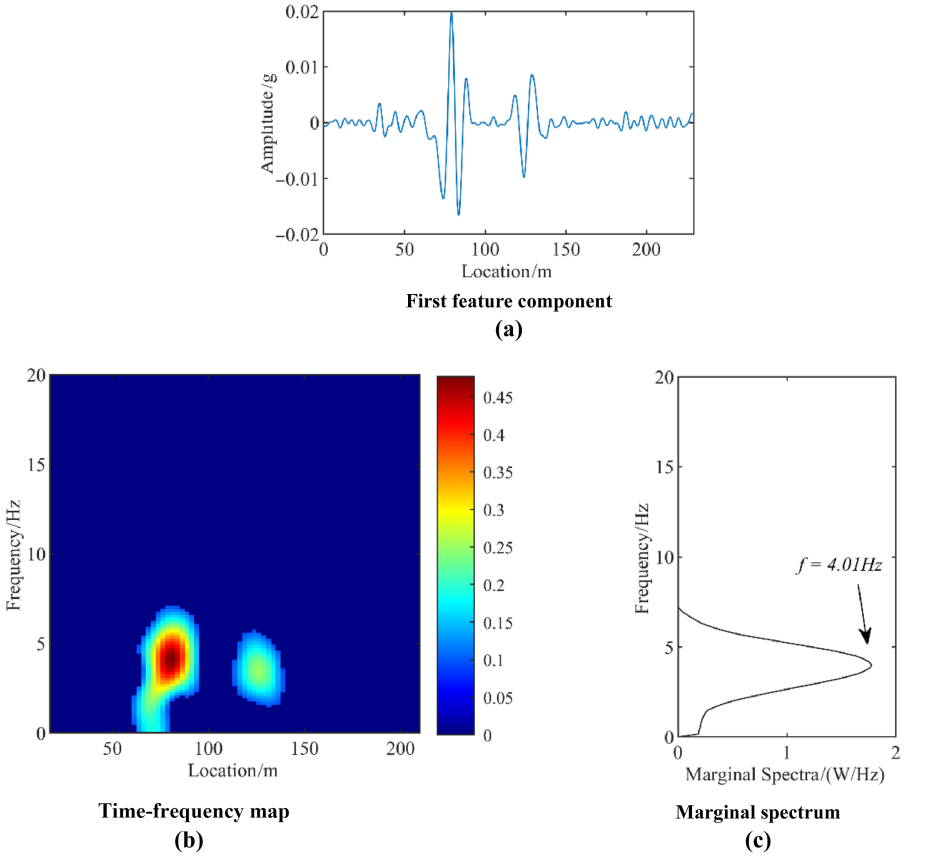

Source(s): Authors' own work

Figure 5. The STFT of no hunting

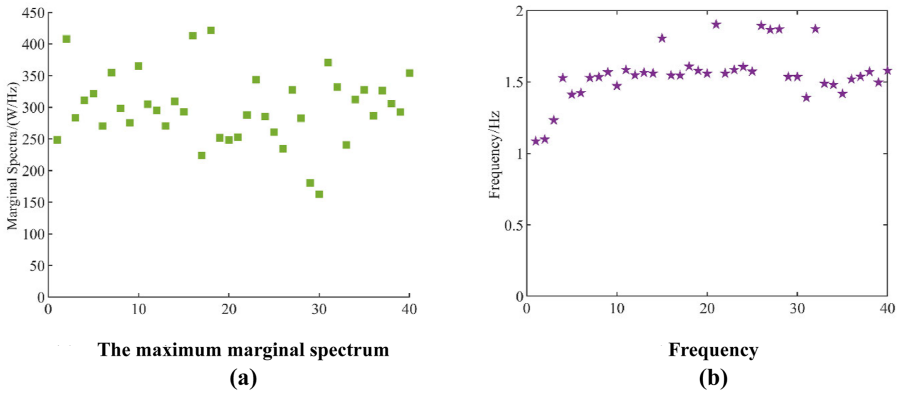

Source(s): Authors' own work

Figure 6. Maximum marginal spectrum and corresponding frequency of hunting

Step 1: Obtain the car body's lateral acceleration in the turnout section;

Step 2: Perform CEEMDAN on the data;

Step 3: Determine the IMF with the highest peak as the first feature component;

Step 4: Perform STFT on the first feature component;

Step 5: Calculate the marginal spectrum;

Step 6: Extract the maximum marginal spectrum value and corresponding frequency.

If the maximum marginal spectrum value and corresponding frequency are consistent with the hunting characteristics, it is determined that the high-speed EMUs have experienced hunting when passing through the turnout.

4. The application of PE in rapid screening of hunting

This is a daunting task to analyze an extensive dataset, exceeding 100,000 entries, which has been compiled from high-speed EMUs as they traverse through turnout areas.

If the proposed diagnostic method is directly applied, it will take a long time. In order to save analysis time, a search method for possible hunting sections based on permutation entropy has been proposed.

4.1 Amplitude and phase

When high-speed EMUs experience periodic hunting through turnouts, the car body's lateral acceleration exhibits obvious periodic characteristics. In this case, car body's lateral acceleration can be simply expressed as

$$A = a\sin(2\pi f \times t + \tau) \tag{15}$$

where a is the amplitude of the car body's lateral acceleration, f is the frequency of periodic hunting, t is the sampling time, and τ is phase.

When collecting data for high-speed comprehensive inspection trains, it is completed through spatial sampling. Therefore, there is a relationship between the sampling time t and the sampling distance x as follows:

$$t = \frac{x}{v} \tag{16}$$

where v is the speed.

Now, four simulation signals have been established to discuss the influence of amplitude a and phase τ on the value of permutation entropy. The signals are shown in Figure 7 and the description is shown in Table 3.

According to the calculation results of permutation entropy, the amplitude and phase values do not affect the permutation entropy value.

4.2 Speed and frequency

According to the result in the previous section, the theoretical car body's lateral acceleration simulation signal constructed can be represented as

$$A = \sin\left(2\pi \times f \times \frac{x}{v}\right) \tag{17}$$

For formula (17), the simulation signal needs to consider the speed v and the frequency f.

At present, high-speed turnouts can be divided into two categories based on management speed: 250 (excluding)-350 km/h management standard high-speed turnouts and 200-250km/h management standard high-speed turnouts. Considering the actual speed of in-service EMUs passing through turnouts, v is taken as 200 km/h, 250 km/h, and 300 km/h.

The lateral vibration frequency of high-speed EMUs passing through turnouts is influenced by multiple factors such as wheel load transition state and high-speed train model coupling.

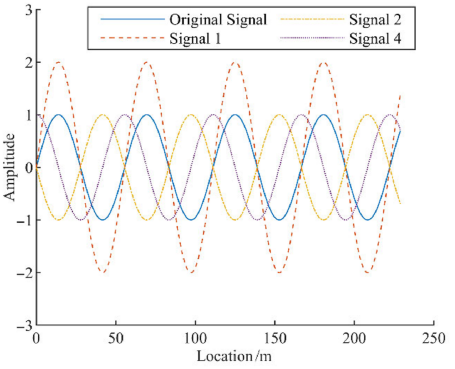

Source(s): Authors' own work

Figure 7. Simulated signals with different amplitudes and phases

Table 3. Signal description

Name	a	τ	Description	PE
Original signal	1	0	/	0.7429
Comparison signal 1	2	0	Different amplitudes and same phase	0.7429
Comparison signal 2	−1	0	Different amplitudes and phases	0.7429
Comparison signal 3	1	$\pi/2$	Same amplitude but different phases	0.7429

Source(s): Authors' own work

There are differences when different high-speed trains pass through different turnout sections. Considering that the lateral vibration frequency is relatively small and generally distributed in the range of 1–2 Hz, f is taken as 1.0 Hz, 1.5 Hz and 2.0 Hz.

Figure 8 shows the simulated signals with the same speed but different frequencies, and with the same frequency at different speeds.

According to Figure 8 (a), at the same speed, the higher the frequency, the longer the vibration period of the vibration signal measured by distance at the same distance, and the fewer vibration waves it contains. According to Figure 8 (b), at the same frequency, the higher the speed, the longer the vibration period of the vibration signal measured by distance at the same distance, and the fewer vibration waves it contains.

Calculate the permutation entropy values for the 9 simulated signals mentioned above, and the results are shown in Table 4.

According to the calculation results, when the frequency is constant, the higher the operating speed, the smaller the value of permutation entropy. When the speed is constant, the higher the frequency, the smaller the value of permutation entropy.

In order to analyze the relationship between permutation entropy and speed, as well as permutation entropy and frequency, multiple simulation signals were established for calculation, and the results are shown in Figure 9. From Figure 9 (a), the maximum value of permutation entropy is 0.7929, corresponding to a frequency of 1.9 Hz; The minimum value of permutation entropy is 0.7429, corresponding to a frequency of 1.0 Hz. At the same speed, as the frequency increases, the overall arrangement entropy value shows a upward trend. There is a significant linear positive correlation between the permutation entropy value and the frequency. The figure shows the linear fitting results for all points except

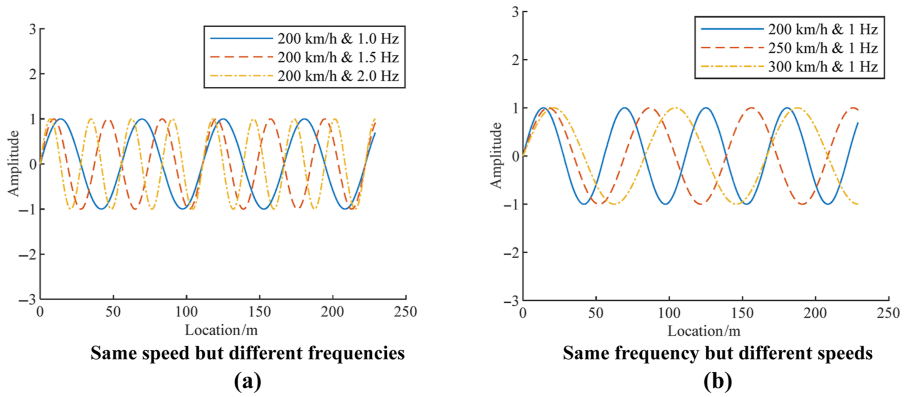

Source(s): Authors' own work

Figure 8. Simulated signals with different speeds and frequencies

Table 4. The permutation entropy of signals with different speeds and frequencies

f \ v	200 km/h	250 km/h	300 km/h
1.0 Hz	0.7429	0.7413	0.7226
1.5 Hz	0.7627	0.7533	0.7429
2.0 Hz	0.7806	0.7774	0.7665

Source(s): Authors' own work

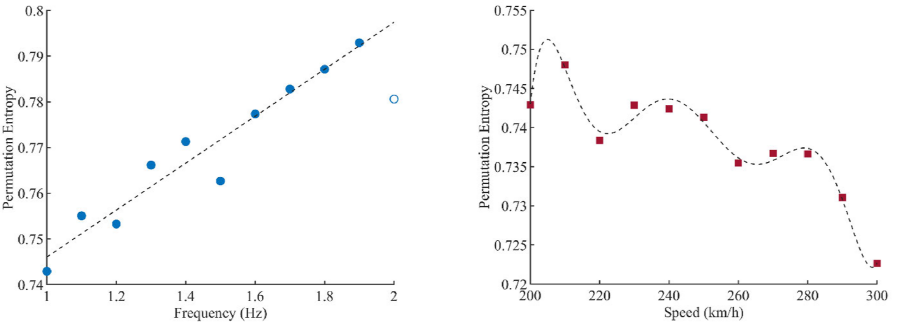

Source(s): Authors' own work

Figure 9. The permutation entropy of simulated signals with different speeds and frequencies

2.00 Hz, with R^2 of 0.9307 and RSME of 0.012. From Figure 9 (b), the maximum value of permutation entropy is 0.7480 and corresponding speed of 210 km/h. The minimum value of permutation entropy is 0.7226 and corresponding speed of 300 km/h. At the same frequency, as the speed increases, the overall arrangement entropy value shows a downward trend. The figure shows the fitting results of a 7th degree polynomial, with the R^2 is 0.9831 and the RMSE is 0.0028.

4.3 Permutation entropy parameter

4.3.1 Embedding dimension. Table 5 shows the time taken to calculate the permutation entropy for the same length signal at the same time delay and different embedding dimension.

As the value of m increases, the calculation time of permutation entropy also increases. When m is less than 5, the calculation response time is around ten milliseconds; when $m = 5$, the calculated response time increases fourfold, reaching 40 milliseconds; when $m = 6$, the calculated response time increases by nearly four times, reaching 140 milliseconds; when $m = 7$, the calculated response time increases by more than 7 times, approaching 1 second; when $m = 8$, the calculation time exceeds 7 seconds; when $m = 9$, the calculation time exceeds 1 minute; when $m = 10$, the calculation time exceeds 10 minutes.

Figure 10 shows the permutation entropy of simulated signals at different embedding dimensions with the same time delay.

From Figure 10 (a) and (b), As m increases, the permutation entropy of simulated signals at the same speed but different frequencies, as well as simulated signals at the same frequency but different speeds, all increase linearly. The larger the value of m, the more significant the difference between different periodic signals. In contrast, periodic signals with different frequencies and the same speed are more sensitive to the value of m than periodic signals with different speeds and the same frequency.

Table 5. Calculation time corresponding to different m

m	3	4	5	6	7	8	9	10
Time/s	0.0140	0.0183	0.0443	0.1482	0.9246	7.1649	64.6325	664.9731

Source(s): Authors' own work

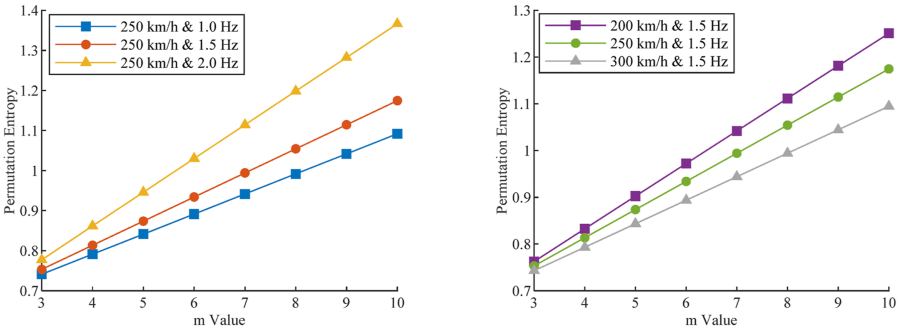

Same speed but different frequencies

(a)

Same frequency but different speeds

(b)

Source(s): Authors' own work

Figure 10. The permutation entropy of simulated signals under different *m* values

Table 6 shows the theoretical maximum permutation entropy and 250 km/h&1 Hz permutation entropy corresponding to different *m*. The value of periodic signal permutation entropy is small.

Table 6. Theoretical maximum PE and 250 km/h&1 Hz PE corresponding to different *m*

m	3	4	5	6	7	8	9	10
Maximum PE	1.0986	1.3863	1.6094	1.7918	1.9459	2.079	2.1972	2.3026
250km/h&1Hz PE	0.7413	0.7913	0.8413	0.8914	0.9415	0.9916	1.0418	1.0920
Ratio	0.67	0.57	0.52	0.50	0.48	0.48	0.47	0.47

Source(s): Authors' own work

4.3.2 Time delay. Table 7 shows the time it takes to calculate the permutation entropy of the same length signal under the same embedding dimension and different time delays. The efficiency is roughly the same under different time delays.

Figure 11 shows the permutation entropy of simulated signals at different time delays with the same embedding dimension.

From Figure 11 (a) and (b), as τ increases, the permutation entropy of simulated signals with the same speed but different frequencies, as well as analog signals with the same frequency but different speeds, increases approximately linearly. There are differences between signals of different periods under different τ values, but they are not significant. In contrast, periodic signals with different frequencies and the same speed are more sensitive to the value of τ than periodic signals with different speeds but the same frequency.

Table 7. Calculation time corresponding to different τ

τ	1	2	3	4	5	6
Time/s	0.1461	0.1447	0.1425	0.1418	0.1407	0.1403

Source(s): Authors' own work

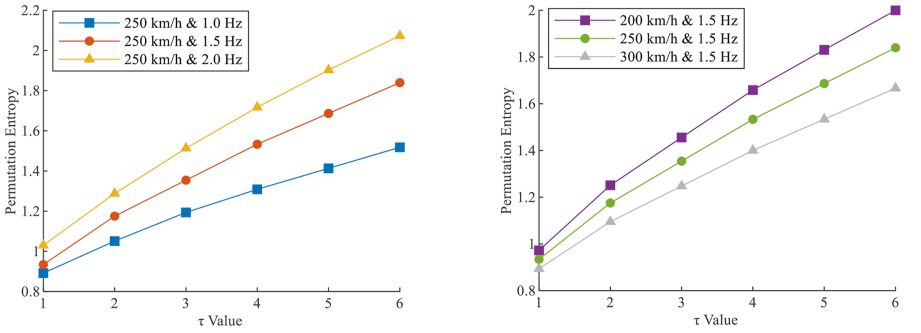

Same speed but different frequencies
(a)

Same frequency but different speeds
(b)

Source(s): Authors' own work

Figure 11. The permutation entropy of simulated signals under different τ values

4.4 The rapid screening method based on PE

The above analysis indicates that periodic signals have lower permutation entropy due to their lower degree of chaos. Therefore, permutation entropy can be used to represent the degree of chaos in the car body's lateral acceleration signal, indirectly reflecting its periodic strength. Considering that the application of permutation entropy in diagnosis is aimed at screening possible problem segments, based on the discussion of key parameters and fully considering computational efficiency, take $m = 3$ and $\tau = 1$. On this basis, the entropy of the lateral acceleration arrangement of 40 sets of hunting and no hunting was analyzed, and the result is shown in Figure 12. The permutation entropy used for analysis of hunting is less than 0.85, and the permutation entropy used for analysis of no hunting is greater than 0.90. Therefore, before conducting diagnosis, the permutation entropy of the car body's lateral acceleration can be calculated first. If the permutation entropy is less than 0.90, it is judged that there may be a problem, and then diagnosis can be carried out with the method proposed.

This operation can significantly improve computational efficiency. Table 8 shows the calculation time of permutation entropy and the diagnostic method proposed. The diagnostic time is 380 times that of calculating Permutation Entropy.

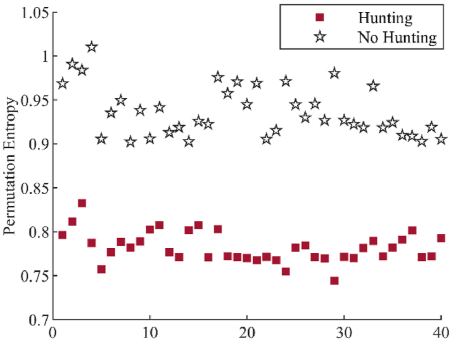

Source(s): Authors' own work

Figure 12. The permutation entropy of hunting and no hunting

Table 8. Calculation time for an acceleration sequence

Name	Calculation time
Permutation entropy	0.0140 *s*
Diagnostic method proposed	5.3243 *s*

Source(s): Authors' own work

5. Experimental validation

A certain CRH2A high-speed EMUs passed through various turnouts and a total of 8,011 pieces of car body's lateral acceleration data were collected in 2023. The analysis results are shown in Table 9. Applying PE < 0.90 to search for possible hunting, 446 pieces of data were determined to be potentially hunting. Using diagnostic methods, the car body's lateral acceleration corresponding to 21 turnouts was determined as hunting. The hunting rate is 0.26%.

The permutation entropy of the data shown in Figure 13 is 0.83, suggesting a potential hunting section. However, upon examining the original waveform, it is observed that the high-speed train did not undergo continuous hunting when passing through the turnout.

After performing CEEMDAN, the first feature component is extracted, as shown in Figure 14 (a). Following this, STFT is applied to obtain the marginal spectrum, and the result is shown in Figure 14 (b) and (c). The maximum marginal spectrum value is 26 W/Hz, corresponding to a frequency of 1.35 Hz, which is notably lower than the range of marginal spectral values associated with continuous hunting of the vehicle body. Consequently, the hunting did not occur.

Table 9. Calculation time for an acceleration sequence

Name	Number
All data	8,011
Possible hunting by PE	446
Hunting by diagnostic methods proposed	21

Source(s): Authors' own work

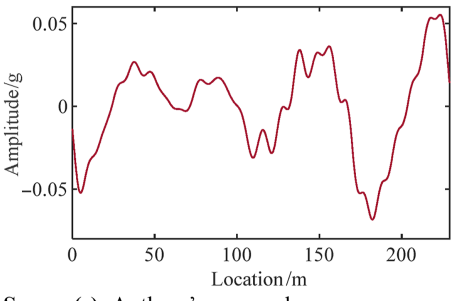

Source(s): Authors' own work

Figure 13. Data judged as possible hunting

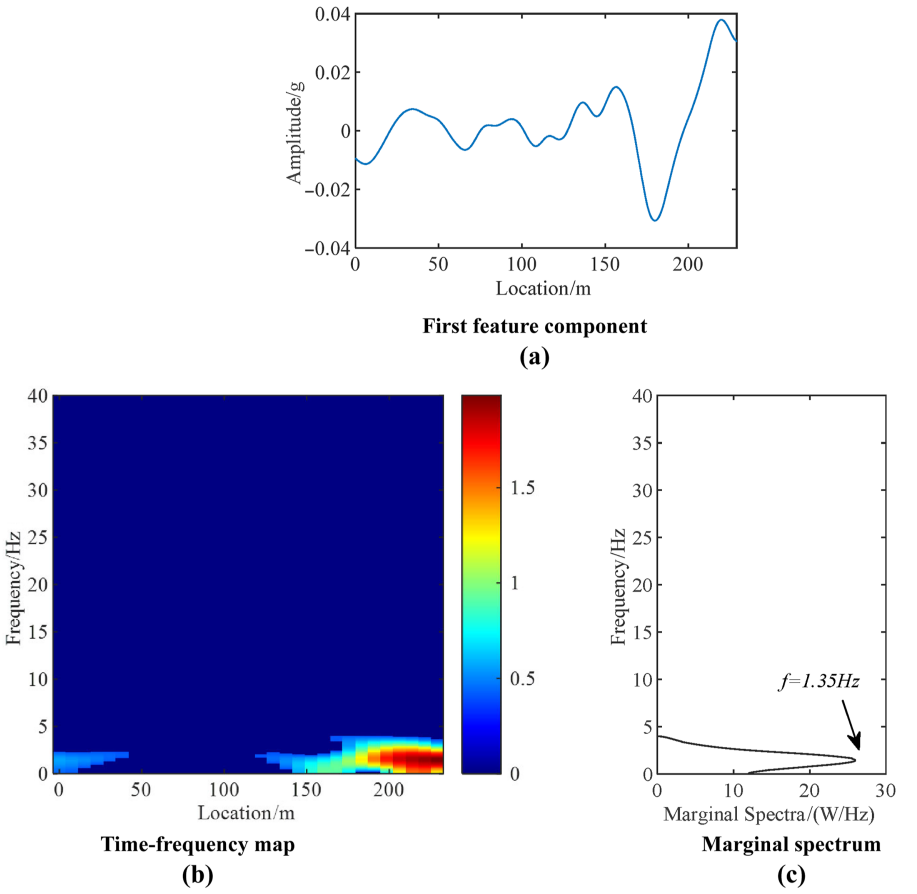

Source(s): Authors' own work

Figure 14. The STFT results of data

6. Conclusion

In this paper, we selected typical representatives of hunting and no hunting when the trains pass through the turnout area. Based on the CEEMDAN results, the IMF with the highest peak value was taken as the research object, and the time-frequency characteristics were analyzed using STFT, which showed that: for hunting, the ratio of the maximum peak value of the signal component to the original signal peak value exceeded 0.7, and there was an energy band in the STFT time-frequency map, which corresponds to a frequency distribution range of 1–2 Hz; for no hunting, the ratio of the maximum peak value of the signal component to the original signal peak value was less than 0.7. The selected typical no hunting data's STFT time-frequency plot showed a circular distribution of energy, with the maximum marginal spectrum corresponding to a frequency of 4.01 Hz.

Based on these data features, we proposed a hunting diagnosis method in turnout area that combined CEEMDAN and STFT. In order to further improve computational efficiency, we discussed the possibility of PE in screening potential problems. By establishing simulation signals, it was found that for periodic signals of the same frequency, the PE corresponding to different amplitudes and phases was the same; periodic signals of different frequencies had

differences in PE; as the embedding dimension m increases, the PE calculation time increased rapidly; the PE calculation time was not sensitive to the value of time delay τ. Considering the computational efficiency of extracting suspicious hunting, took $m = 3$ and $\tau = 1$. At this point, the permutation entropy of hunting used for analysis was less than 0.85 and the permutation entropy of hunting without hunting used for analysis was greater than 0.9. Thus, a PE value of 0.90 can be used as the judgment criterion to determine the possibility of hunting. At this point, each PE calculation took only 0.0140 s, which was 1/380 of the proposed diagnostic method's 5.3243 s. Finally, the rapid diagnostic method was applied to analyze the hunting of the CRH2A high-speed EMUs in the turnout section in 2023, which showed a hunting rate of 0.20%. In further analysis, we will attempt to investigate the causes of this hunting.There are three points worthy of further study: (1) By collecting and analyzing data from different types of high-speed trains, the aim should be to understand the differences in the hunting of the car body when passing through turnouts for different types of high-speed trains. (2) The change in wheel tread state will affect the equivalent taper between the wheel and rail, which in turn will affect the lateral stability of the vehicle system. In the future, the relationship between the hunting of the car body and the mileage of the wheels should be quantitatively analyzed. (3) The mechanism of hunting when a high-speed train passes through a turnout has not been conclusively determined, so the next step should be to explore this in conjunction with vehicle system dynamics.

References

Cheng, D., Wen, Y., Guo, Z., Hu, X., Wang, P., & Song, Z. (2024). Research on the evolution law of dynamic performance of CR400BF EMU train based on stochastic dynamics simulation. *Railway Sciences*, *2*(2), 143–155. doi: 10.1108/rs-01-2024-0004.

Chi, M., Zhang, W., Zeng, J., Jin, X., & Zhu, M. (2008). Influence of hunting motion on ride quality of railway vehicle. *Journal of Vibration Engineering*, *21*(6), 639–643.

Cong, J., Zhang, H., Wei, Z., Yang, F., Ke, Z., Lu, T., ... Li, Z. (2024). Estimation of speed-related car body acceleration limits with quantile regression. *Railway Sciences*, *3*(5), 575–592. doi: 10.1108/rs-06-2024-0019.

Deng, C., Zhou, J., Xia, Z., Gong, D., & Sun, Y. (2020). Online detection and control of high-speed train's low-frequency swaying. *Journal of Tongji University*, *48*(3), 441–446.

Gao, Y., Si, D., Wang, S., & Yang, D. (2023). Influence of wheel-rail profile evolution on contact geometric relationship in turnout. *China Railway Science*, *44*(5), 169–179.

Garrido, M. (2016). The feedforward short-time fourier transform. *IEEE Transactions on Circuits and Systems Part II: Express Briefs*, *63*(9), 868–872. doi: 10.1109/tcsii.2016.2534838.

Guo, J., Zhang, G., Shi, H., & Zeng, J. (2023). Small-amplitude bogie hunting identification method for high-speed trains based on machine learning. *Vehicle System Dynamics*, *62*(5), 1253–1267. doi: 10.1080/00423114.2023.2224906.

Huang, N. E., Shen, Z., Long, S. R., Wu, M. C., Shih, H. H., Zheng, Q., ... Liu, H. (1998). The empirical mode decomposition and the Hilbert spectrum for nonlinear and non-stationary time series analysis. In *Proceedings of the Royal Society of London Series A* (Vol. 454(1971), pp. 903–995). doi: 10.1098/rspa.1998.0193.

Kaewunruen, S. (2014). Monitoring structural deterioration of railway turnout systems via dynamic wheel/rail interaction. *Case Studies in Nondestructive Testing and Evaluation*, *1*(1), 19–24. doi: 10.1016/j.csndt.2014.03.004.

Kang, H., Zhang, X., & Zhang, G. (2020). Phase permutation entropy: A complexity measure for nonlinear time series incorporating phase information. *Physica A: Statistical Mechanics and its Applications*, *568*, 125686. doi: 10.1016/j.physa.2020.125686.

Li, J., Ding, J., Li, F., Niu, Y., & Yang, Y. (2020). High-speed turnout vehicle dynamics index research and vehicle dynamics calculation. *Railway Standard Design*, *64*(10), 157–162.

Li, H., Zhao, J., Liu, B., Zhao, G., Sheng, L., & Zhang, Z. (2021). Research on technical route of inspection and monitoring system for high-speed railway infrastructure. *China Railway*, *1*, 98–104.

Liu, J. (2016). Discussion of the swaying of carbodies. *Rolling Stock*, *54*(2), 33–35, 6.

Luo, R., & Shi, H. (2018). *Dynamics of railway vehicle systems and application*. Chengdu: Southwest Jiaotong University Press.

Ma, X., Wang, P., Wang, J., & Xu, J. (2016). Study on impact of over-limit reduced value of switch rail on dynamic characteristics of switch. *Journal of the China Railway Society*, *38*(3), 98–105.

Ning, J., Cui, W., Chong, C., Ouyang, H., Chen, C., & Zhang, B. (2018). Feature recognition of small amplitude hunting signals based on the MPE-LTSA in high-speed trains. *Measurement*, *131*, 452–460. doi: 10.1016/j.measurement.2018.08.035.

Niu, D. (2020). Technology and development of railway infrastructure lifetime inspection. *Railway Engineering*, *60*(4), 5–8, 16.

Niu, D., Ke, Z., Liu, W., Li, H., Zhao, G., & Liu, X. (2020). Research on the inspection and monitoring system framework of high-speed railway infrastructure. *China Railway*, *10*, 9–17.

Qin, H., Liu, J., Wang, W., & Sun, S. (2019). An expeditious computational method for twice correction of mileage deviation from vehicle dynamic response inspection data. *China Railway Science*, *40*(4), 112–119.

Shi, D., Sabanovic, E., Rizzetto, L., Skrickij, V., Oliverio, R., Kaviani, N., . . . Hecht, M. (2022). Deep learning based virtual point tracking for real-time target-less dynamic displacement measurement in railway applications. *Mechanical Systems and Signal Processing*, *166*, 108482. doi: 10.1016/j.ymssp.2021.108482.

Sun, J., Meli, E., Cai, W., Gao, H., Chi, M., Rindi, A., & Liang, S. (2021). A signal analysis based hunting instability detection methodology for high-speed railway vehicles. *Vehicle System Dynamics*, *12*(10), 1461–1483. doi: 10.1080/00423114.2020.1763407.

Sun, S., Wang, W., Liu, J., & Li, H. (2012). Study of carbody's severe vibration based on stability analysis of vehicle system. *China Railway Science*, *33*(2), 82–88.

Torres, M. E., Colominas, M. A., Schlotthauer, G., & Flandrin, P. (2011). A complete ensemble empirical mode decomposition with adaptive noise. In *IEEE International Conference on Acoustics, Speech and Signal Processing* (pp. 4144–4147) New York: IEEE.

Wang, P. (2016). *Design of high-speed railway turnouts theory and applications*. Chengdu: Southwest Jiaotong University Press.

Wang, S., Si, D., Wang, M., & Ge, J. (2014). Influence of value reduced for switch rail of high-speed railway on riding quality. *China Railway Science*, *35*(3), 28–33.

Wang, S., Wang, P., Ge, J., Si, D., & Yang, D. (2022). Study on wear characteristics and management limit of switch rail in high-speed turnout. *China Railway Science*, *43*(1), 9–16.

Wang, P., Wang, S., Ge, J., Si, D., & Yang, D. (2023). Study on wear characteristics and authorized limits of switch rails of high-speed turnout. *Railway Sciences*, *2*(2), 157–169. doi: 10.1108/rs-03-2023-0014.

Wang, M., Ning, J., Zhao, F., Li, Y., & Chen, C. (2023). Hunting classification method based on HHT energy and largest lyapunov exponent. *Computer Measurement & Control*, *31*(8), 169–175.

Wei, L. (2016). *Study on related running safety problems for high-speed trains*. Chengdu: Southwest Jiaotong University.

Wu, Z., & Huang, N. E. (2009). Ensemble empirical mode decomposition: A noise-assisted data analysis method. *Advances in Adaptive Data Analysis*, *1*(1), 1–41. doi: 10.1142/s1793536909000047.

Xia, Z., Zhou, J., Gong, D., Sun, W., & Sun, Y. (2018). Research on low-frequency lateral sway of railway vehicle body based on modal continuous tracking. *Journal of the China Railway Society*, *40*(12), 46–54.

Xie, W. (2022). Research on track service state evaluation method based on bogie lateral displacement. PhD thesis, Beijing: China Academy of Railway Sciences.

Xie, W., Liu, J., Zhao, G., Zhou, Z., Liu, W., & Diao, H. (2022). Analysis and diagnosis of low frequency periodic shaking of high speed EMU. *Railway Engineering*, *62*(2), 1–4.

Xie, W., Qin, H., Qi, Z., Yang, F., Zhao, G., & Mao, X. (2024). Evaluation and pattern research of high speed turnout track geometry. *China Railway*, *3*, 25–31.

Yang, F., Wang, P., Sun, J., & Wang, S. (2020). The law of switch rail wear in high-speed turnout and its effect on dynamic performance. *Journal of Railway Engineering Society*, *37*(3), 13–20, 66.

Ye, Y., & Ning, J. (2019). Small-amplitude hunting diagnosis method for high-speed trains based on the bogie frame's lateral-longitudinal-vertical data fusion, independent mode function reconstruction and linear local tangent space alignment. In *Proceedings of the Institution of Mechanical Engineers, Part F: Journal of Rail and Rapid Transit*, *233*(10), 1050–1067. doi: 10.1177/0954409718825412.

Ye, Y., Ning, J., Zhong, C., Cui, W., & Liu, Q. (2016). Feature analysis of high-speed train bogie hunting instability based on modified ensemble empirical mode decomposition and Hilbert transformation. *China Measurement & Test*, *42*(9), 120–125.

Ye, Y., Ning, J., Zhong, C., Cui, W., & Liu, Q. (2017). Hunting instability of high-speed train diagnose method based on modified ensemble empirical mode decomposition Shannon entropy and LSSVM. *Application Research of Computers*, *34*(4), 1097–1100.

Ye, Y., Ning, J., Zhong, C., Cui, W., & Chen, C. (2018). Forecasting model of hunting instability of high-speed train bogie based on Modified Ensemble Empirical mode decomposition and least squares support vector machine. *Journal of the China Railway Society*, *40*(1), 38–43.

Zhang, E., Zhang, M., Wu, Q., Niu, L., Xia, C., & Sun, S. (2021). Development and application of portable axle box acceleration detection system. *Railway Engineering*, *61*(3), 151–154.

Zheng, J., Pan, H., Yang, S., & Cheng, J. (2018). Generalized composite multiscale permutation entropy and Laplacian score based rolling bearing fault diagnosis. *Mechanical Systems and Signal Processing*, *99*, 229–243. doi: 10.1016/j.ymssp.2017.06.011.

Corresponding author
Jinzhao Liu can be contacted at: liujinzhao@rails.cn